Submitted to The Astrophysical Journal

Three-Dimensional Magnetohydrodynamic Simulations of Spherical Accretion

Igor V. Igumenshchev[1,2] and Ramesh Narayan
Harvard-Smithsonian Center for Astrophysics, 60 Garden Street, Cambridge MA 02138

ABSTRACT

We present three-dimensional numerical magnetohydrodynamic simulations of radiatively inefficient spherical accretion onto a black hole. The simulations are initialized with a Bondi flow, and with a weak, dynamically unimportant, large-scale magnetic field. The magnetic field is amplified as the gas flows in. When the magnetic pressure approaches equipartition with the gas pressure, the field begins to reconnect and the gas is heated up. The heated gas is buoyant and moves outward, causing line stretching of the frozen-in magnetic field. This leads to further reconnection, and more heating and buoyancy-induced motions, so that the flow makes a transition to a state of self-sustained convection. The radial structure of the flow changes dramatically from its initial Bondi profile, and the mass accretion rate onto the black hole decreases significantly.

Motivated by the numerical results, we develop a simplified analytical model of a radiatively inefficient spherical flow in which convective transport of energy to large radii plays an important role. In this "convection-dominated Bondi flow" the accretion velocity is highly subsonic and the density varies with radius as $\rho \propto R^{-1/2}$ rather than the standard Bondi scaling $\rho \propto R^{-3/2}$. We estimate that the mass accretion rate onto the black hole correspondingly scales as $\dot{M} \sim (R_{in}/R_a)\dot{M}_{Bondi}$, where R_{in} is a small multiple of the Schwarzschild radius of the black hole and R_a is the "accretion radius" at which the ambient gas in the surrounding medium is gravitationally captured by the black hole. Since the factor R_{in}/R_a is typically very small, $\dot{M}$ is significantly less than the Bondi accretion rate. Convection-dominated Bondi flows may be relevant for understanding many astrophysical phenomena, e.g. post-supernova fallback and radiatively inefficient accretion onto supermassive black holes, stellar-mass black holes and neutron stars.

Subject headings: accretion — convection — galaxies: nuclei — MHD — supernovae — turbulence

[1]Laboratory for Laser Energetics, University of Rochester, 250 East River Road, Rochester NY 14623-1299.

[2]Institute of Astronomy, 48 Pyatnitskaya Ulitsa, 109017 Moscow, Russia.

1. Introduction

The classic problem of adiabatic spherical accretion onto a compact gravitating mass has been studied by many authors. The hydrodynamic version of this problem was solved by Bondi (1952) who showed that inside a certain capture radius, the radial velocity of the accreting gas varies as $v_R \propto R^{-1/2}$, where R is the radius. Correspondingly, the density varies as $\rho \propto R^{-3/2}$.

If the gas in a Bondi flow has a frozen-in magnetic field, the field lines are stretched in the radial direction and compressed in the transverse direction, so that the radial component of the field is amplified according as $B_R \propto R^{-2}$. The magnetic energy density then varies as $\epsilon_m = B^2/8\pi \propto R^{-4}$. However, the gravitational energy density of the gas varies only as $\epsilon_{grav} = \rho GM/R \propto R^{-5/2}$. Thus, for a sufficiently small radius, one formally has $\epsilon_m \gg \epsilon_{grav}$, which is physically inconsistent since the magnetic energy ultimately is derived from the gravitational binding energy of the accreting gas.

Shvartsman (1971) proposed that the conversion of gravitational energy into magnetic energy is accompanied by turbulence which tangles the magnetic field lines. He suggested that, as the magnetic and gravitational energies approach equipartition, field reconnection ensures that ϵ_m does not exceed ϵ_{grav}. Reconnection will be accompanied by dissipation (Bisnovatyi-Kogan & Ruzmaikin 1974; Mészáros 1975) which will heat the gas. As a result, the thermal energy of the gas is also likely to come into rough equipartition with the other energies. These modifications have been recognized for many years and have been incorporated into models of spherical accretion flows.

To our knowledge, all published studies of the magnetized spherical accretion problem have assumed that the magnetic field causes no serious *dynamical* effects on the flow. In particular, all authors assume that the velocity and density scale exactly as in the Bondi solution, namely $v_R \propto R^{-1/2}$, $\rho \propto R^{-3/2}$. (The following is an incomplete list of relevant papers on the subject: Zeldovich & Novikov 1971; Shapiro 1973a,b; Ipser & Price 1977, 1982, 1983; Maraschi et al. 1979; Maraschi, Roasio, & Treves 1982; Scharlemann 1981, 1983; Treves, Maraschi, & Abramowicz 1988; Turolla & Nobili 1989; Nobili, Turolla, & Zampieri 1991; Mason & Turolla 1992; Mason 1992; Melia 1992; Kowalenko & Melia 1999; Coker & Melia 2000; many other papers discuss spherical accretion without explicitly considering magnetic fields and heating, e.g. Ostriker et al. 1976; Park & Ostriker 1989; Houck & Chevalier 1991; Zampieri et al. 1998.)

In this paper we show that the magnetic field can play an important, perhaps even dominant, role in the dynamics of spherical accretion flows. The influence is both direct, through the action of the electromotive force, and indirect, through the entropy generated in the process of field reconnection. The latter leads to convection, which drastically changes the flow structure relative to the Bondi solution. In particular, the density profile becomes much less centrally peaked than the Bondi $R^{-3/2}$ profile, and the mass accretion rate is reduced significantly below the Bondi rate. Interestingly, the flow resembles the recently discovered hydrodynamical convection-dominated accretion flow solution (CDAF, Narayan, Igumenshchev, & Abramowicz 2000; Quataert &

Gruzinov 2000; Stone, Pringle, & Begelman 1999; Igumenshchev & Abramowicz 2000, 2001; Igumenshchev, Abramowicz, & Narayan 2000; Ball, Narayan, & Quataert 2001).

The rest of the paper is organized as follows. In §2 we describe our numerical method, and the details of our initial and boundary conditions. In §3 we present results of numerical simulations, and in §4 we describe an approximate self-similar solution which includes the effects of plasma heating and convection. In §5 we discuss some implications of the results.

2. Simulation Technique

2.1. Magnetohydrodynamic Equations

We solve the equations of resistive MHD in the one-fluid approximation,

$$\frac{d\rho}{dt} + \rho\nabla\cdot\mathbf{v} = 0, \tag{1}$$

$$\rho\frac{d\mathbf{v}}{dt} = -\nabla(P+Q) - \rho\nabla\Phi + \frac{1}{4\pi}(\nabla\times\mathbf{B})\times\mathbf{B}, \tag{2}$$

$$\rho\frac{d\epsilon}{dt} = -(P+Q)\nabla\cdot\mathbf{v} + \frac{1}{4\pi}\eta\mathbf{J}^2, \tag{3}$$

$$\frac{\partial\mathbf{B}}{\partial t} = \nabla\times(\mathbf{v}\times\mathbf{B} - \eta\mathbf{J}), \tag{4}$$

where ρ is the density, $\mathbf{v}$ is the velocity, P is the pressure, Φ is the gravitational potential, $\mathbf{B}$ is the magnetic induction, ϵ is the specific internal energy, $\mathbf{J}=\nabla\times\mathbf{B}$ is the current density, and η is the resistivity. The terms involving Q in equations (2) and (3) correspond to an artificial viscosity which is introduced to correctly treat shocks. We adopt the ideal gas equation of state,

$$P = (\gamma-1)\rho\epsilon, \tag{5}$$

with an adiabatic index $\gamma = 5/3$. We assume that there is no radiative cooling.

We take the compact mass at the center to be a black hole of mass M and we use a pseudo-Newtonian gravitational potential (Paczyński & Wiita 1980) to mimic the effects of general relativity,

$$\Phi = -\frac{GM}{R-R_g}, \qquad R_g = \frac{2\,GM}{c^2}, \tag{6}$$

where R_g is the gravitational radius.

2.2. Numerical Method

We numerically solve equations (1)–(4) by using an extension of the original PPM algorithm developed by Colella & Woodward (1984) for hydrodynamics. We use the Lagrangian version of

the PPM algorithm with operator splitting. The Riemann solver takes into account the non-linear interaction of the fast MHD waves when calculating time-updates of the density, velocity and internal energy in equations (1)–(3). The components of the Lorentz force in the equation of motion (2) are calculated using a solution of the Lagrangian characteristic equations for Alfvén waves, as in the method of characteristics (MOC) of Stone & Norman (1992). We use dimension splitting when solving the equations in three dimensions.

We replace the induction equation (4) by an equivalent equation for the vector potential $\mathbf{A}$,

$$\frac{\partial \mathbf{A}}{\partial t} = \mathbf{v} \times \mathbf{B} - \eta \mathbf{J}, \tag{7}$$

where $\mathbf{B} = \nabla \times \mathbf{A}$. This approach guarantees that the constraint $\nabla \cdot \mathbf{B} = 0$ is satisfied to within grid approximation errors at each time t. The first term on the right hand side of equation (7) is calculated using a modified version of the Eulerian MOC algorithm (Stone & Norman 1992). (The modification is due to our use of a different representation of the location of the Alfvén characteristics domain for calculating the averaged values of the components of $\mathbf{v}$ and $\mathbf{B}$.)

The code operates on a three-dimensional Cartesian grid. In order to adequately resolve the large dynamic range of spatial scales spanned by astrophysical accretion flows, we employ a nested grid (see Fig. 1) similar to that employed by Igumenshchev et al. (2000) for simulating hydrodynamical CDAFs in three dimensions. In the present calculations, we have used five subgrids with $64 \times 64 \times 64$ cells in each subgrid. The cell size in the innermost subgrid is $\Delta_1 = 0.5R_g$. Each succeeding subgrid has its cell size increased by a factor of 2, and so the outermost subgrid has $\Delta_5 = 8R_g$, and covers a cube of size $256R_g \times 256R_g \times 256R_g$. In practice, we used only a quarter of the full cubic domain, by focusing on a 90 degree wedge around the z axis. Thus, we employed $32 \times 32 \times 64$ cells along xyz, and used periodic boundary conditions in the azimuthal direction.

We define the quantities ρ, $\rho\mathbf{v}$ and $\rho\epsilon$ at the centers of cubic cells, and the components of $\mathbf{B}$ at the corresponding cell edges. By using continuous piece-wise parabolic approximations of $\mathbf{v}$ and $\mathbf{B}$ when solving equation (7), the code avoids the "explosive" instability which is found in MHD codes based on the original MOC algorithm (Clarke 1996).

The energy equation in numerical MHD needs to be handled with care. Because of the finite spatial resolution, field lines can reconnect, leading to a loss of magnetic energy without a compensating increase in the internal energy of the gas. This leads to uncontrolled energy loss in the simulation (e.g. Stone & Pringle 2001; Igumenshchev & Abramowicz 2001).

To fix the problem, we introduce an explicit artificial resistivity η and set its magnitude to be larger than the effective numerical resistivity associated with numerical reconnection. Following Stone & Pringle (2001), we choose

$$\eta = \eta_0 \frac{|\nabla \times \mathbf{B}|}{\sqrt{4\pi\rho}} \Delta^2, \tag{8}$$

where η_0 is a dimensionless parameter and Δ is the grid spacing. The magnetic Reynolds number

corresponding to this resistivity is

$$Re_m \simeq \frac{1}{\eta_0}\left(\frac{L}{\Delta}\right)^2, \tag{9}$$

where L is the characteristic spatial scale of the problem.

Ryu, Jones, & Frank (1995) have shown that the effective Reynolds number due to numerical resistivity has the same functional dependence on L and Δ as in equation (9), and they estimate the corresponding coefficient $(\eta_0)_n$ to be in the range $0.2 - 0.5$ for their second-order MHD code based on the total variation diminishing scheme. We expect that our code has the same or even lower numerical resistivity. For this reason, we have used η_0 in the range of $0.3 - 0.5$. Test runs show a significant improvement in energy conservation when we choose η_0 in this range.

In principle, the non-uniform nested numerical grid (Fig. 1) could introduce perturbations in the flow at the interfaces between subgrids because of differences in the numerical viscosity and resistivity on the two sides of the boundary. We checked for this effect in rotating hydrodynamical accretion flows (Igumenshchev et al. 2000), and found that the perturbations were small and had no significant effect on the global flow. The present simulations of MHD accretion flows again show only minor effects at sub-grid interfaces.

2.3. Initial and boundary conditions

We initialize our simulations with a spherically symmetric flow, described by the following self-similar Bondi solution for a $\gamma = 5/3$ gas in the Newtonian gravitational potential of a point mass M,

$$\rho(R) = \frac{\dot{M}}{4\pi}\frac{R^{-3/2}}{v_0\sqrt{GM}}, \quad v_R(R) = -v_0\sqrt{\frac{GM}{R}}, \quad \epsilon(R) = \frac{3}{5}\left(1 - \frac{v_0^2}{2}\right)\frac{GM}{R}, \tag{10}$$

where $\dot{M}$ is the mass accretion rate and v_0 is a dimensionless parameter which can take any value in the range $0 \le v_0 \le \sqrt{2}$. In all our simulations we have taken $v_0 = 1$, which corresponds to supersonic Bondi accretion with Mach number $\mathcal{M} = 1.7$. We take the initial magnetic field to be uniform with only one non-zero component: B_z. We specify the initial strength of the magnetic field B_z by a parameter b_0 defined as follows,

$$\frac{B_z^2}{8\pi} = b_0^2\frac{GM\rho_{out}}{R_{out}}, \tag{11}$$

where ρ_{out} is the density of the gas at the outer radius of the grid $R_{out} = 256\,R_g$. We choose $b_0^2 \ll 1$, which ensures that the magnetic field has negligible influence on the flow dynamics early in the simulation.

At the outer boundary we assume that, at all times, the density and the velocity are given by the Bondi solution (10) and the magnetic field is equal to its initial value. At the inner boundary, close to the black hole horizon, we assume absorbing conditions. Specifically, any matter that

crosses the inner radius $R_{in} = 2R_g$ is extracted from the computational domain, and the magnetic terms in the equation of motion (2) are switched off.

3. Numerical Results

We have calculated four models, A, B, C, D, with the parameters listed in Table 1. All the models begin with a weak magnetic field ($b_0^2 \ll 1$), which has a negligible dynamical effect on the flow. Therefore, the spherical Bondi solution with which the flow is initialized is stable and persists for some time. As the gas flows in, the strength of the magnetic field increases, with the most rapid increase occurring in the innermost region. At a certain critical time the field becomes strong enough to modify the flow dynamics.

Figure 2 shows the evolution of the mass accretion rate onto the black hole for Models A (thin line), B (dashed line) and D (thick line). At the beginning of the simulations the accretion rates in all three models experience a quick relaxation. This initial relaxation is due to the fact that there is a minor inconsistency between the self-similar solution (10) and the absorbing inner boundary conditions as well as the pseudo-Newtonian potential (6). At the end of the initial relaxation, the flow takes up a slightly modified steady state configuration, and the mass accretion rate onto the black hole becomes equal to the rate of mass input at the outer boundary. At this point, the flow is essentially the standard Bondi flow. Model D, which is a pure hydrodynamic simulation, does not change any further after this initial relaxation. Models A, B and C, however, which have magnetic fields, undergo significant evolution.

Figure 3 shows the configuration of magnetic field lines in Model A at time $t = 0.5$; we measure time in units of the free-fall time from the outer radius R_{out} of the computational domain. We see that the initially parallel field lines are pulled in towards the black hole as they are swept in by the converging flow streamlines. Note that, near the equatorial plane, oppositely directed magnetic lines closely approach each other. This leads to efficient reconnection soon after this time.

At $t \simeq 0.5$ in Model A the strength of the magnetic field in the vicinity of the black hole reaches equipartition with the gas pressure, and the accretion rate experiences a sudden large drop. This drop represents the effect of the amplified magnetic field, which suppresses accretion in the equatorial zone and forces matter to accumulate within a "core" region in the vicinity of the black hole. Because the initial Bondi flow is supersonic, an MHD shock forms where the inflowing matter meets the core. The post-shock gas is sub-sonic and sub-Alfvenic. In Model B the same drop in accretion rate is again seen, except that it happens at a later time ($t \approx 1$). This model starts with a weaker field and therefore it takes longer for the magnetic pressure to build up to equipartition strength. Model C, with a smaller value of the resistivity parameter η_0, has an evolution almost identical to that of Model A. All three models relax to a new state in which the mass accretion rate is several times less than the mass supply rate. The accretion rates in

Models A, B and C continue to evolve slowly with time and by the end of the simulations ($t \sim 8$), the rates are roughly an order of magnitude less than the mass supply rate. The accretion rates are highly variable, however, reflecting the unstable nature of the flows. All three models have very similar final states.

Here we discuss Model A in detail as a representative example. As already mentioned, a dense core is formed in the innermost region of the accretion flow once the magnetic field reaches equipartition with the gas pressure. The core is bounded by a quasi-spherical shock. The size of the core and the mass contained in it increase with time due to the accumulation of matter; matter flows onto the core from the outside at a rate determined by the rate of mass input at the outer boundary, while mass flows out of the core into the black hole at a much lower rate (roughly a factor of ten lower).

Figures 4, 5 and 6 show the distribution of density, magnetic field lines and velocity streamlines in the core region at a relatively late time, $t = 7.88$. The influence of the large scale magnetic field introduced through the outer boundary condition is still visible in the polar direction. The magnetic field here is almost radial and has its maximum strength. Correspondingly, the density takes its minimum value, so that the plasma $\beta \equiv P_g/P_m$ is quite small, $\beta \sim 0.1$. The accreting matter moves along the magnetic lines with supersonic velocity; the velocity is roughly of order the Alfven speed. Because of the high velocity there is no accumulation of matter.

As Figures 4–6 show, the picture is very different in the equatorial region ("equator" and "pole" are defined with respect to the large-scale magnetic field). The topology of the magnetic field is much more tangled and the gas is denser. The accumulated matter is highly inhomogeneous, with filaments of higher and lower density being sandwiched between each other (Fig. 4). The inhomogeneous structure is the result of convection in the core driven by the heat released during episodes of magnetic reconnection.

The first reconnection event occurs at a time slightly later than that shown in Figure 3. The reconnection and corresponding energy release happens exactly at the equatorial plane, in the vicinity of the inner boundary, where the magnetic field is strongest and where oppositely directed field lines approach each other most closely. After the reconnection event the local strength of the magnetic field is reduced to a sub-equipartition level (as visualized by Shvartsman 1971) and the gas is heated by the energy released in the reconnection. The heated gas expands and forms a convective blob which moves outward as a result of buoyancy force. During the motion of the hot blob through the ambient medium it deforms magnetic lines and causes new reconnection events. This leads to the formation of other hot blobs which again become convective. As a result, the convective motions are self-sustained and lead to turbulence in the core. The magnetic field in the convection zone is on average close to equipartition strength, with $\beta \simeq 1$–10.

Figure 5 shows the tangled magnetic field configuration after the convection has become fully developed, and Fig. 6 shows the chaotic velocity streamlines. We see numerous vortices and circulation patterns. The most efficient convection occurs at intermediate angles between the

poles and the equator. Somewhat less efficient convective motions are present in the equatorial plane, and there is no convection in the polar regions.

4. Self-Similar Solutions

To better understand the physics of radiatively inefficient magnetized spherical accretion, we consider here a steady radial flow and seek self-similar solutions of the equations. By the assumption of self-similarity, we expect the plasma β to be independent of radius R. Hence we write the gas, magnetic and total pressure as

$$P_g \equiv \rho c_s^2, \qquad P_m = \frac{1}{\beta}\rho c_s^2, \qquad P_{tot} = P_g + P_m = \frac{\beta+1}{\beta}\rho c_s^2, \tag{12}$$

where c_s is the isothermal sound speed of the gas. The radial momentum equation and the gas energy equation take the form

$$\frac{d}{dR}\left(\frac{v_R^2}{2}\right) = -\frac{1}{\rho}\frac{dP_{tot}}{dR} - \frac{GM}{R^2}, \tag{13}$$

$$\rho v_R T \frac{ds}{dR} \equiv \rho v_R \left[\frac{1}{\gamma-1}\frac{dc_s^2}{dR} - \frac{c_s^2}{\rho}\frac{d\rho}{dR}\right] = -\frac{1}{R^2}\frac{d}{dR}(R^2 F_c) + Q_{diss}, \tag{14}$$

where v_R is the radial velocity (assumed negative for accretion), s is the specific entropy of the gas, γ is the adiabatic index, and F_c is the outward flux of energy due to convection. The term on the left hand side of equation (14) describes the inward advection of energy, the first term on the right hand side is the divergence of the convective energy flux, and Q_{diss} is the rate of heating of the gas by dissipation.

Following Narayan & Yi (1994, see also Kato, Fukue, & Mineshige 1998; Narayan et al. 2000), we use a simple parametric form to represent the convective flux,

$$F_c = -\alpha_c c_s R \rho T \frac{ds}{dR}, \tag{15}$$

where α_c is a dimensionless constant. For the heating term, Q_{diss}, we note that there are at least two sources of dissipation: (i) energy release through magnetic reconnection, and (ii) viscous and resistive dissipation at small scales as a result of a turbulent cascade. It is not possible to model these processes in detail. Instead, we note that the ultimate source of energy is the gravitational potential energy of the accreting gas, and so we write

$$Q_{diss} = -\alpha_d \frac{v_R}{R}\rho\frac{GM}{R}, \tag{16}$$

where α_d is another dimensionless constant (the negative sign is because $v_R < 0$).

We consider self-similar flows in which the various variables behave as power laws in radius (see the analogous discussion of CDAFs in Narayan et al. 2000),

$$c_s(R) = c_0 v_K \propto R^{-1/2},$$

$$\rho(R) = \rho_0 R^{-a}, \tag{17}$$

$$v_R(R) = \frac{\dot{M}}{4\pi R^2 \rho} = -v_0 v_K \left(\frac{R_g}{R}\right)^{(3/2-a)} \propto R^{-2+a},$$

where $v_K = \sqrt{GM/R}$ is the Keplerian velocity, and a is a power-law index which takes one of two values, 3/2 or 1/2 (see Narayan et al. 2000 and Quataert & Gruzinov 2000). The coefficients c_0 and v_0 are dimensionless coefficients whose values are determined by substituting the solution into the two conservation equations (13) and (14). The coefficient ρ_0 is proportional to the accretion rate $\dot{M}$ and scales out of the problem.

The simplest case to consider is the pure hydrodynamic problem, in which gas with $\gamma = 5/3$ accretes onto a black hole, with neither convection nor dissipative heating. The self-similar solution with $a = 3/2$ automatically satisfies the energy equation, while the momentum equation gives

$$v_0^2 = 2 - \frac{5(\beta+1)}{\beta} c_0^2. \tag{18}$$

We then have a family of solutions in which v_0 is a free parameter and c_0 is determined by equation (18) (with $\beta \to \infty$ since there is no magnetic field),

$$c_0^2 = \frac{1}{5}(2 - v_0^2). \tag{19}$$

This is the self-similar solution given in equation (10), which was used to initialize the numerical simulations. The same self-similar solution is often used even for magnetized spherical accretion, under the assumption that the field will achieve equipartition and thereby have a self-similar scaling. But this is not correct. When there is a magnetic field, there is bound to be reconnection (see the discussion in §1) and this means that the entropy of the gas will increase inward. This is not consistent with the assumed scaling ($a = 3/2$, $\gamma = 5/3$, cf. Quataert & Narayan 1999).

In the presence of magnetic fields, we need to consider the more general problem with finite values of β, α_c and α_d, and a general value of γ. Let us first assume that a takes the standard Bondi value of 3/2. In this case, all the terms in the energy equation (14) are of the same order (all scale as R^{-4}), and the energy equation gives the following relation between v_0 and c_0,

$$\left(\frac{1}{\gamma - 1} - \frac{3}{2}\right)(v_0 - \alpha_c c_0) c_0^2 = \alpha_d v_0. \tag{20}$$

This relation, combined with equation (18) from the momentum equation, allows us to solve uniquely for v_0 and c_0 for given values of β, α_c, α_d and γ. However, not all combinations of these

parameters lead to a physical solution. For instance, consider the case when $\alpha_c c_0 \ll v_0$. Equation (20) then gives

$$c_0^2 = \frac{\alpha_d}{\left(\frac{1}{\gamma-1} - \frac{3}{2}\right)}, \tag{21}$$

which shows that γ has to be less than 5/3 if c_0^2 is to be positive and finite. In fact, the constraint on γ is even more severe. This can be seen by substituting (21) in (18) and solving for v_0^2. The requirement that $v_0^2 > 0$ leads to

$$\frac{1}{\gamma-1} > \frac{3}{2} + \frac{5(\beta+1)\alpha_d}{2\beta}, \tag{22}$$

which gives an upper limit on γ that is smaller than 5/3.

The reason for these constraints is that the value $\gamma = 5/3$ is a singular case for a self-similar solution with $a = 3/2$. This fact was noted by Quataert & Narayan (1999) for the case of a rotating viscous flow, but the same argument applies here as well. When the condition $\alpha_c c_0 \ll v_0$ which was used to derive (21) is not satisfied, the inequality (22) becomes modified to a more complicated relation. However, the qualitative features remain the same. Specifically, we find that γ has to be smaller than a certain value (which is less than 5/3) in order to have a physical solution.

Let us next consider a self-similar solution with $a < 3/2$. Now, the various terms in the energy equation are no longer of the same order. The entropy advection term and the heating term still vary as R^{-4}, but the term describing the divergence of the convective flux varies as $R^{-5/2-a}$. The latter term dominates at large R. Since there is no other term to balance this term, the only way to satisfy the energy equation is to ensure that its coefficient is equal to zero. This requires $a = 1/2$.

Let us now set $a = 1/2$. As we have just argued, the energy equation is automatically satisfied (to leading order) at large R. The momentum equation also becomes simpler since the term involving v_R is smaller than the other two terms and may be neglected. Thus we find

$$c_0^2 = \frac{2\beta}{3(\beta+1)}. \tag{23}$$

The value of the parameter v_0 is not uniquely determined by this analysis, but is fixed by boundary conditions. In particular, close to the black hole, where the various terms in the energy equation become of comparable order (in fact, the convective term probably becomes less important than the other two terms), the flow will make a transition to a different regime; this is also the region where the flow matches onto the absorbing boundary condition at the black hole. We do not discuss the physics of this region as it is beyond the scope of the present paper.

A feature of the $a = 1/2$ self-similar solution is that $\gamma = 5/3$ is not a singular case (the solution is singular when $\gamma = 3$, but this has no practical consequences). Thus, for an accretion flow with $\gamma = 5/3$, the $a = 1/2$ solution appears to be more robust than the $a = 3/2$ solution. For

lower values of γ, both the $a = 3/2$ solution and the $a = 1/2$ flow may be allowed and it is not a priori obvious which solution would be picked by nature. We suspect that the $a = 1/2$ solution is the flow of choice under most conditions (see also the discussion of the $a = 1/2$ law by Gruzinov 2001).

The two solutions discussed above are very different from each other. In the $a = 3/2$ flow, convection is a relatively minor perturbation and the energy balance is primarily between energy advection and dissipative heating. This flow is very similar to the standard Bondi accretion flow, with only minor changes in the values of some coefficients. In contrast, in the new $a = 1/2$ solution, the convective flux dominates the energy equation. We therefore refer to it as a convection-dominated Bondi Flow (CDBF). This flow deviates remarkably from the standard Bondi solution; in fact, it resembles the CDAF solution.

The CDBF has a steady outward flux of energy due to convection. The convective luminosity is

$$L_c = 4\pi R^2 F_c = \frac{\alpha_c c_0^3}{2v_0}\left(\frac{1}{\gamma-1}-\frac{1}{2}\right)\dot{M}c^2 \equiv \varepsilon_c \dot{M}c^2. \tag{24}$$

Thus, convection transports a fraction of the binding energy of the accreting gas outward. The efficiency of this process, described by the coefficient ε_c, depends on details of the flow which are not easy to determine from first principles. In the case of a CDAF, where again there is an analogous relation, numerical simulations by Igumenshchev & Abramowicz (2000; see also Narayan et al. 2000; Igumenshchev et al. 2000) give $\varepsilon_c \sim 0.001 - 0.01$. It is likely that a CDBF also has a similar efficiency.

5. Summary and Discussion

The main result of this paper is that radiatively inefficient spherical (i.e. non-rotating) accretion of magnetized plasma onto a compact mass has very different properties compared to spherical accretion of unmagnetized gas. The unmagnetized problem is described by pure hydrodynamics. It was solved by Bondi (1952) and has been widely applied.

Our results on the magnetized problem are based on three-dimensional numerical MHD simulations. The simulations are initialized with an analytical self-similar Bondi flow (eq. [10]) and have initially a weak, dynamically unimportant magnetic field ($b_0^2 \ll 1$, cf eq. [11]). The inner boundary conditions correspond to a black hole. We find that the Bondi solution survives for a short period of time with relatively minor changes. However, during this time the magnetic field becomes progressively stronger — because of radial stretching and transverse compression of the frozen-in field lines as the gas flows in — until the magnetic pressure builds up roughly to equipartition with the gas pressure (Figure 3).

After this time, the structure of the flow changes dramatically. The equipartition magnetic field exerts a back-reaction on the free-falling gas and slows it down in the "equatorial" region. A

shock forms and gas accumulates in a "core." The magnetic field begins to reconnect to maintain the magnetic pressure slightly below equipartition (plasma $\beta \sim 1 - 10$). The reconnection heats the gas locally, and the resulting high entropy material moves outward under buoyancy. The outward motion causes further stretching and amplification of the frozen-in field lines, leading to further episodes of reconnection. Before long, the plasma in the vicinity of the black hole experiences fully developed turbulent convection. With time, the convective core grows in size, as more magnetized material from the outside is added to it, while mass flows into the black hole at a much smaller rate. The flow in the convective core bears almost no resemblance to the Bondi solution (see Figures 4, 5 and 6). One result of all this is that the accretion rate onto the black hole is reduced significantly from the Bondi rate (Figure 2). The flow does not have a wind or outflow, as in the models of Blandford & Begelman (1999) and Das (2000), but this is not surprising since those authors include additional ingredients such as angular momentum and viscosity (Blandford & Begelman, see also Narayan & Yi 1994) and pair physics (Das).

The principal physical effects operating in our numerical simulations may be understood by considering the energetics of the accreting magnetized plasma. We can identify three major stages in which the gravitational binding energy of the accreting gas is transformed into other forms of energy:

(gravitational energy)

$\downarrow$

(magnetic energy)

$\downarrow$

(thermal energy)

$\downarrow$

(convective turbulent energy, leading to convective energy transport)

The first and second transformations, namely (gravitational energy)→(magnetic energy) and (magnetic energy)→(thermal energy) are well-known and have been widely discussed (Shvartsman 1971; Bisnovatyi-Kogan & Ruzmaikin 1974; Mészáros 1975; and numerous later papers, see §1). These two processes build up the magnetic field to near-equipartition strength and modify the thermal state of the gas (and its radiative properties) relative to the standard Bondi flow. However, they have little effect on the overall dynamics of the flow.

The third transformation, (thermal energy)→(convective turbulence), does have a very important effect on the dynamics, and this appears to have been overlooked in previous studies. The importance of convection is not because it creates turbulent kinetic energy (which is just another form of pressure, like magnetic and thermal pressure), but because it causes energy *transport*. Convection efficiently transports energy from the deep interior of the flow, where the bulk of the gravitational energy is released, to the outer regions of the flow. Away from the center,

the convective flux dominates the physics and thus has a significant effect on the structure of the flow.

In the MHD simulations presented here, the mass accretion rate onto the black hole is reduced by a factor of about ten relative to a Bondi flow with the same outer boundary conditions (of density and sound speed). The reduction occurs because of the formation of the convective core. The mean accretion velocity in the core is highly subsonic, and much smaller than the radial velocity in an equivalent Bondi flow. Only very close to the inner absorbing boundary does the accretion become supersonic, in contrast to a standard Bondi flow which has supersonic infall over a wide range of radius. The radial density profile is also very different from the $R^{-3/2}$ profile found in a Bondi flow.

We should caution that, in our models, we have assumed that the external medium has a uniform magnetic field. This leads to a large departure from spherical symmetry in the accretion flow at late times. For instance, Figures 4–6 show a bipolar structure in the magnetic field, with two "poles" (oriented parallel to the external field) along which there is preferential accretion. The situation we have simulated would be realized if the coherence scale of the field in the external medium is larger than the accretion radius R_a — the radius at which the gas from the external medium is captured by the gravitational pull of the accreting mass. However, one could visualize other situations in which the field is tangled on small scales in the external medium, so that the accreting gas has several distinct magnetic loops.

We have tried numerical experiments on accretion flows with small scale magnetic field of different configurations. However, we lacked sufficient numerical resolution for these experiments; the field underwent resistive dissipation before it could reach equipartition with the gas pressure. This demonstrates the importance of having adequate numerical resolution. We estimate that to conduct any believable experiments with a non-uniform external field we will need to increase the numerical resolution by a factor of at least 2–3.

Despite the above cautionary comment, the basic physical ideas we have presented should be valid whatever be the topology of the field; namely, line stretching and field amplification leads to reconnection, which leads to gas heating, which leads to convection. This chain of argument requires merely that the magnetic field should be frozen into the gas and that the magnetic field should build up to equipartition strength before the gas falls into the black hole. Since the magnetic pressure grows as R^{-4} whereas the gas pressure varies only as $R^{-5/2}$ (§1), the latter condition should be easily satisfied in most cases of interest.

Another cautionary comment is related to the fact that our simulations have not reached steady state. The convective core grows slowly and has reached a size of only about $80R_g$ by the end of our simulations. This is still a factor of 3 smaller than the size of the grid. In a real accretion flow we imagine that the convective core would grow until it extends beyond R_a. The convective flux would then flow out into the external medium, and perhaps modify the medium in the vicinity of R_a. Ultimately, a steady state should result, but the present simulations have not

been run long enough to determine the nature of the steady state.

In §4 we present a simplified set of equations to describe spherical accretion of a magnetized plasma. The equations include two critical pieces of physics: (i) heating of the gas by reconnection (and other dissipative processes), and (ii) convective energy transport. Depending on parameters, we find that there are two distinct self-similar solutions of the equations.

One solution is not very different from the standard Bondi solution; the density varies as $\rho \propto R^{-3/2}$ and the velocity varies as $v_R \propto R^{-1/2}$. This solution is possible whenever convection is not very strong and when the adiabatic index γ of the gas is smaller than a limit which is less than the standard value of 5/3 (cf. discussion below eqs [21, 22]). For given boundary conditions at the accretion radius R_a, the mass accretion rate in this solution is similar to the Bondi accretion rate $\dot{M}_{Bondi}$. Our numerical simulations, however, are not consistent with this solution. At this time we are not sure if the solution is relevant for any radiatively inefficient spherical accretion flow with strong fields.

The second solution is completely different from the Bondi solution. It has density varying as $\rho \propto R^{-1/2}$ and velocity varying as $v_R \propto R^{-3/2}$. The scalings may be understood as follows.

The bulk of the energy generation in the accretion flow happens close to the black hole. Some fraction of this energy is transported outward by convection. At radii greater than a certain transition radius R_{in}, whose value is uncertain but is probably no more than a few tens of R_g, the convective luminosity L_c completely dominates over any local energy generation. Thus, for $R > R_{in}$, we expect L_c to be practically independent of R; equivalently, the convective flux F_c must vary as R^{-2}. Because the accretion flow is assumed to be radiatively inefficient, the gas is virial and has a sound speed $c_s \sim v_K$ (the Kepler or free-fall velocity). Thus, there is only one velocity in the problem, namely $v_K \propto R^{-1/2}$; therefore, the convective flux has to take the form $F_c \sim \rho c_s^3 \sim \rho v_K^3 \sim \rho R^{-3/2}$. Requiring the convective flux to vary as R^{-2} means that ρ must scale as $R^{-1/2}$. Mass conservation, $\dot{M} = -4\pi R^2 v_R \rho =$ constant, then immediately gives $v_R \propto R^{-3/2}$. Thus, the structure of the flow is determined uniquely once we assume (i) that there is a significant flux of energy outward due to convection, and (ii) that there is no significant radiative cooling.

Because of the important role played by convection, we refer to this kind of flow as a convection-dominated Bondi flow, or CDBF. The scalings sketched out above allow us to estimate the mass accretion rate in this flow. In the standard Bondi problem, where a mass M is embedded in a homogeneous medium of density ρ_∞ and sound speed c_∞, the accretion radius is given by $R_a \sim GM/c_\infty^2$; this is the radius at which the gravitational free-fall velocity is equal to c_∞. The gas in the Bondi solution flows in at essentially the free-fall velocity for $R \lesssim R_a$; therefore, the mass accretion rate is given by $\dot{M}_{Bondi} \sim 4\pi R_a^2 \rho_\infty c_\infty$. In a CDBF, we expect v_R to be roughly equal to the free-fall velocity at $R \sim R_{in}$. Since v_R falls off as $R^{-3/2}$, this means that at $R \sim R_a$, v_R is smaller than the local free-fall velocity by a factor $\sim R_{in}/R_a$. We then estimate that

$$\dot{M}_{CDBF} \approx \frac{R_{in}}{R_a} \dot{M}_{Bondi}. \tag{25}$$

This shows that convection can have a profound effect on the mass accretion rate in a magnetized spherical accretion flow.

The convective core region in the simulations presented in this paper (Figures 4, 5 and 6) have features that are qualitatively similar to the predictions of the self-similar CDBF solution. Unfortunately, due to limited spatial resolution, we have not been able to make quantitative comparisons between the numerical results and the predictions of the analytical model. The averaged radial profiles of density, velocity, gas and magnetic pressures show significant oscillations, both in space and time. They also show the influence of the inner boundary (black hole) and outer boundary (the shock where the free-falling gas meets the convective core), which cannot be separated out because of the relatively small range of radius covered by the simulations. More extensive numerical work is required to confirm the theoretical predictions in detail. Also, in a real flow, we expect the CDBF zone to extend all the way out to R_a, where it would match the ambient density ρ_∞ and ambient pressure $\rho_\infty c_\infty^2$ of the external medium. The simulations have not reached steady state. This is another reason why it is difficult to compare the numerical results with the theoretical predictions.

We should note the close analogy between the CDBF solutions described here and the viscous rotating (non-magnetic) CDAF solution (Narayan et al. 2000; Quataert & Gruzinov 2000). The CDAF is more complex because, in addition to the radial momentum equation and the energy equation, it is also strongly influenced by the angular momentum equation. In particular, there is a competition between viscosity and convection in the angular momentum balance, which plays an important role in determining the structure of the solution. Nevertheless, the particular radial scalings seen in a CDAF, $\rho \propto R^{-1/2}$, $v_R \propto R^{-3/2}$, are identical to those found in a CDBF, and they result from the same physics identified above, namely the presence of an energetically dominant convective flux and the absence of radiative cooling. Furthermore, the accretion rate in a CDAF is reduced compared to that in an equivalent advection-dominated accretion flow (ADAF, cf. Narayan & Yi 1994; Abramowicz et al. 1995), for the same outer boundary conditions, by a factor $\sim R_{in}/R_{out}$, which is similar to the factor given in equation (25). The exact value of R_{in} in the two problems depends on the nature of the flow close to the black hole. This is discussed in a forthcoming paper (Abramowicz et al. 2001).

We should note a few other numerical experiments we have carried out which provide further insights. First, as already mentioned, when we use too large an artificial resistivity in the simulations, such that the magnetic field reconnects long before it reaches equipartition, we find that the flow does not make a transition to a convection-dominated form. This is not surprising since in this case there is very little heating from reconnection and therefore there is not enough entropy production to drive significant convection. Although it is not fully understood how reconnection works in astrophysical plasmas (but see the recent work of Lazarian & Vishniac 1999), it does seem reasonable to assume that significant reconnection occurs only after the field builds up at least to equipartition strength (as proposed by Shvartsman 1971). If this assumption is valid for real astrophysical flows, then the simulations we have presented, and our analytical

results, should be relevant.

To further investigate the importance of resistive heating, we have carried out a series of simulations in which we set the artificial resistivity η in equations (3) and (4) to zero. In these runs, we find significant magnetic reconnection through numerical resistivity, but there is no corresponding heating of the gas. The flows do not exhibit convection. As in Models A–C described in §3, when the magnetic field reaches equipartition with the gas pressure, a central "core" region is formed, bounded by a quasi-spherical shock. However, the core is more compact and the accretion rate is only slightly reduced with respect to the Bondi rate. The flow pattern in the core is perturbed with respect to the spherical inflow due to the effect of the magnetic field, but the perturbations are not as significant as in Models A–C, and the velocity streamlines are not as chaotic.

To understand how important the magnetic field is for the formation of the convective core, we have carried out three-dimensional hydrodynamic simulations with finite bulk and/or shear viscosity, and with two values of γ: 5/3, 4/3. We expected that the bulk viscosity would heat the accreting gas and that this might lead to efficient convection. Instead, we find that viscous Bondi flows are stable for a wide range of values of the bulk and shear viscosity coefficients. Combined with the experiments described in the previous paragraph, the implication is that both the electromotive forces associated with the magnetic field and the heating effect due to reconnection are important for the flow to become convection-dominated; any one by itself is not enough. Once the CDBF state has been achieved, it appears to be stable and self-sustaining.

We note recent simulations of three-dimensional rotating MHD accretion flows by Hawley, Balbus, & Stone (2001). These flows exhibit the magnetorotational instability, as expected. One might have expected them also to be convective, at least at large radius, and to have a radial structure similar to a CDBF (or a CDAF). However, Hawley et al. (2001) report that they do not observe convective motions in their models. We suspect that this may be because they do not include a resistive heating term. (Stone & Pringle 2001 do include an artificial resistivity, but their simulations are in two dimensions.) In the Hawley et al. simulations, the energy release due to (numerical) reconnection is lost from the system and the total energy is not conserved. As noted above, we have simulated spherical accretion without including an artificial resistivity, and we do not see convection. In this sense, the two studies are consistent.

Accretion flows in many astrophysical systems involve magnetized plasma. We would like to suggest that any astrophysical system that has radiatively inefficient spherical accretion will set up a convection-dominated flow similar to the CDBF solution discussed here, and will behave very differently from the standard Bondi solution. In particular, we suggest that the mass accretion rate will be given by equation (25), which is very much less than the Bondi accretion rate. This has potentially important implications.

In a classic paper, Fabian & Canizares (1988) used the Bondi solution to estimate the mass accretion rate $\dot{M}$ onto supermassive black holes in the nuclei of nearby giant elliptical galaxies

and showed that the observed nuclear luminosities are far below the luminosity expected if the radiative efficiency is the canonical 10%. The problem has become more severe in recent times with improved observations of the nucleus of our own Galaxy (Baganoff et al. 2001) and nuclei of other nearby galaxies (e.g. Di Matteo et al. 2001). One solution to the luminosity problem is to assume that the accretion occurs in a radiatively inefficient mode, e.g. via an ADAF (Narayan, Yi, & Mahadevan 1995; Fabian & Rees 1995; Reynolds et al. 1996). The present work suggests an even simpler solution, namely, the mass accretion rate onto the supermassive black hole may be much less than the Bondi rate assumed by Fabian & Canizares (1988). For conditions typical of galactic nuclei, say $c_\infty \lesssim 10^3$ km s^{-1}, we expect $R_a \sim 10^5 R_g$. Since R_{in} in equation (25) is likely to be no more than a few tens of R_g, we see that $\dot{M}$ with a CDBF could be smaller than $\dot{M}_{Bondi}$ by a large factor $\sim 10^3 - 10^4$.

Another application is to isolated neutron stars and black holes accreting from the interstellar medium in the Galaxy. Treves & Colpi (1991) and Blaes & Madau (1993) used the Bondi accretion rate to estimate the likely luminosities of accreting neutron stars and discussed the possibility of detecting them by their EUV and X-ray emission. A number of later papers have discussed theoretical predictions for the emitted spectrum (e.g. Turolla et al. 1994; Zane, Turolla, & Treves 1996). Despite careful searches in the ROSAT all-sky survey, the predicted large number of sources has not been found (e.g. Belloni, Zampieri, & Campana 1997). As in the case of dim galactic nuclei, we suggest that the discrepancy is because the accretion on the neutron stars occurs via a convection-dominated flow, so that the mass accretion rate is far below the Bondi rate. There are similar implications also for accreting stellar-mass black holes (e.g. Fujita et al. 1998).

Yet another possible application is to supernova explosions. In addition to the prompt collapse of a homologous core, current models of supernovae predict fallback of material over an extended period of time after the explosion (Chevalier 1989). This material, which is ejected with less than the escape speed, flows out radially, turns around at some (large) radius and collapses back on the compact core. Some of this material may experience significant magnetic field amplification and may undergo reconnection and heating. If so, it is likely to develop convective motions, resulting in a much reduced rate of mass fallback. This deserves further study.

We gratefully thank Tom Abel, Marek Abramowicz, Axel Brandenburg and Eliot Quataert for helpful discussions and comments. This work was supported by NSF grant AST 9820686, NASA grant NAG5-10780 and RFBR grant 00-02-16135.

REFERENCES

Abramowicz, M. A., Chen, X., Kato, S., Lasota, J.-P, & Regev, O. 1995, ApJ, 438, L37

Abramowicz, M. A., Igumenshchev, I. V., Narayan, R., & Quataert, E. 2001, in preparation

Baganoff, F. K., et al. 2001, ApJ, in press (astro-ph/0102151)

Ball, G., Narayan, R., & Quataert, E. 2001, ApJ, 552, 221

Belloni, T., Zampieri, L. & Campana, S. 1997, A&A, 319, 525

Bisnovatyi-Kogan, G. S., & Ruzmaikin, A. A. 1974, Astr. Space Sci., 28, 45

Blaes, O., & Madau, P. 1993, ApJ, 403, 690

Blandford, R. D., & Begelman, M. C. 1999, MNRAS, 303, L1

Bondi, H. 1952, MNRAS, 112, 195

Chevalier, R. A. 1989, ApJ, 346, 847

Clarke, D. A. 1996, ApJ, 457, 291

Coker, R., & Melia, F. 2000, ApJ, 534, 723

Colella, P., & Woodward, P. R. 1984, J. Comput. Phys., 54, 174

Das, T. 2000, MNRAS, 318, 294

Di Matteo, T., Johnstone, R. M., Allen, S. W., & Fabian, A. C. 2001, ApJ, 550, L19

Fabian, A. C., & Canizares, C. R. 1988, Nature, 333, 829

Fabian, A. C., & Rees, M. J. 1995, MNRAS, 277, L55

Fujita, Y., Inoue, S., Nakamura, T., Manmoto, T., & Nakamura, K. E. 1998, ApJ, 495, L85

Gruzinov, A. 2001, preprint (astro-ph/0104113)

Hawley, J. F., Balbus, S. A., & Stone, J. M. 2001, preprint (astro-ph/0103522)

Houck, J. C., & Chevalier, R. A. 1991, ApJ, 376, 234

Igumenshchev, I. V., & Abramowicz, M. A. 2000, ApJS, 130, 463

Igumenshchev, I. V., Abramowicz, M. A., & Narayan, R. 2000, ApJ, 537, L27

Igumenshchev, I. V., & Abramowicz, M. A. 2001, in AIP Conf. Proc., 20th Texas Symp. on Relativistic Astrophysics, ed. J. C. Wheeler & H. Martel (New York: AIP), in press (astro-ph/0102482)

Ipser, J. R., & Price, R. H. 1977, ApJ, 216, 578

Ipser, J. R., & Price, R. H. 1982, ApJ, 255, 654

Ipser, J. R., & Price, R. H. 1983, ApJ, 267, 371

Kato, S., Fukue, J., & Mineshige, S. 1998, Black-Hole Accretion Disks (Kyoto: Kyoto Univ. Press)

Kowalenko, V., & Melia, F. 1999, MNRAS, 310, 1053

Lazarian, A., & Vishniac, E. T. 1999, ApJ, 517, 700

Maraschi, L., Perola, G. C., Reina, C., & Treves, A. 1979, ApJ, 230, 243

Maraschi, L., Roasio, R., & Treves, A. 1982, ApJ, 253, 312

Mason, A. 1992, MNRAS, 255, 203

Mason, A. & Turolla, R. 1992, ApJ, 400, 170

Melia, F. 1992, ApJ, 387, L25

Mészáros, P. 1975, A&A, 44, 59

Narayan, R., Igumenshchev, I. V., & Abramowicz, M. A. 2000, ApJ, 539, 798

Narayan, R., & Yi, I. 1994, ApJ, 428, L13

Narayan, R., Yi, I., & Mahadevan, R. 1995, Nature, 374, 623

Nobili, L., Turolla, R., & Zampieri, L. 1991, ApJ, 383, 250

Ostriker, J. P., Weaver, R., Yahil, A., & McCray, R. 1976, ApJ, 208, 61

Paczyński, B., & Wiita, J. 1980, A&A, 88, 23

Park, M.-G., & Ostriker, J. P. 1989, ApJ, 347, 679

Quataert, E., & Narayan, R. 1999, 516, 399

Quataert, E., & Gruzinov, A. 2000, ApJ, 539, 809

Reynolds, C. S., Fabian, A. C., Cellotti, A., & Rees, M. J. 1996, MNRAS, 283, 873

Ryu, D., Jones, T. W., & Frank, A. 1995, ApJ, 452, 785

Scharlemann, E. T. 1981, ApJ, 246, L15

Scharlemann, E. T. 1983, ApJ, 272, 279

Shapiro, S. L. 1973a, ApJ, 180, 531

Shapiro, S. L. 1973b, ApJ, 185, 69

Shvartsman, V. F. 1971, Soviet Astron. J., 15, 37

Stone, J. M., & Norman, M. L. 1992, ApJS, 80, 791

Stone, J. M., Pringle, J. E. & Begelman, M. C. 1999, MNRAS, 310, 1002

Stone, J. M., & Pringle, J. E. 2001, MNRAS, 322, 461

Treves, A., & Colpi, M. 1991, A&A, 241, 107

Treves, A., Maraschi, L., & Abramowicz, M. 1988, PASP, 100, 427

Turolla, R., & Nobili, L. 1989, ApJ, 342, 982

Turolla, R., Zampieri, L., Colpi, M., & Treves, A. 1994, ApJ, 426, L35

Zampieri, L., Colpi, M., Shapiro, S. L., & Wasserman, I. 1998, ApJ, 505, 876

Zane, S., Turolla, R., & Treves, A. 1996, ApJ, 471, 248

Zeldovich, Ya. B., & Novikov, I. D. 1971, Relativistic Astrophysics, Chicago: Univ. of Chicago Press, 1971

Table 1. Parameters of the Models

Model	η_0 [a]	b_0 [b]
A	0.5	0.3
B	0.5	0.1
C	0.3	0.3
D	0	0

[a] η_0 is a dimensionless artificial resistivity parameter, defined in equation (8).

[b] b_0 characterizes the initial magnetic field, and is defined in equation (11).

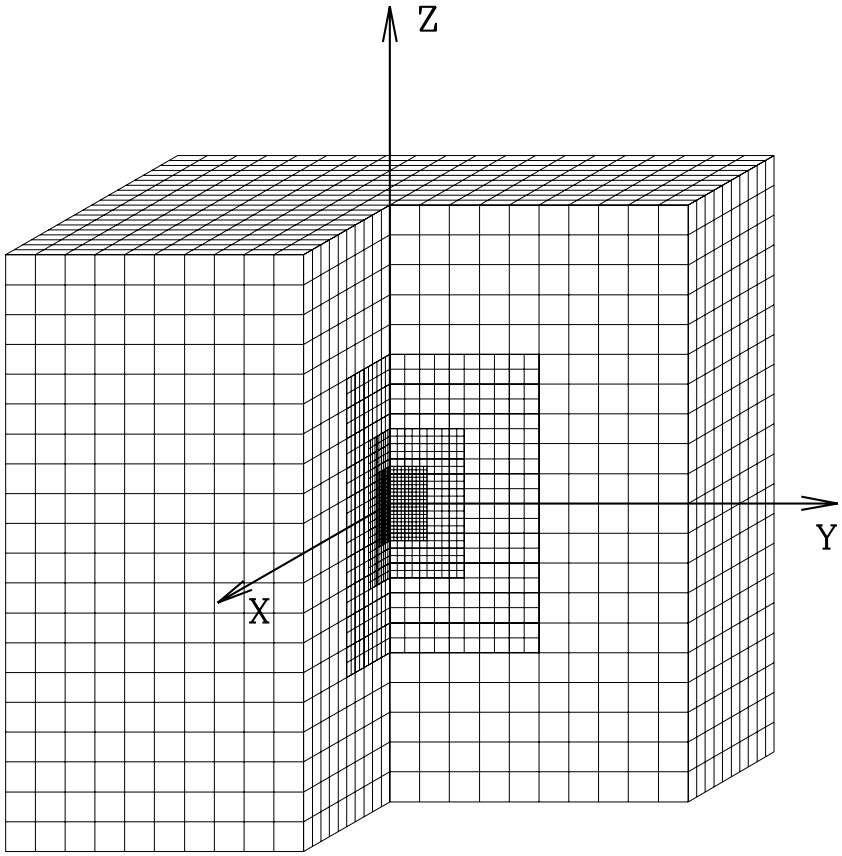

Fig. 1.— Schematic view of the nested Cartesian grid used in the simulations. The example shown has four sub-grids, each of size $20 \times 20 \times 20$. In the actual calculations five sub-grids were used with dimensions $64 \times 64 \times 64$. The black hole is located at the origin.

Fig. 2.— Time evolution of the mass accretion rate, normalized to the Bondi rate, in Model A (thin line), Model B (dashed line) and Model D (thick line). Note the suppression of the accretion rate in Models A and B, both of which have magnetic fields. Model D corresponds to a pure hydrodynamic flow.

Fig. 3.— Magnetic lines in Model A at time $t = 0.5$ (measured in units of the free-fall time from the edge of the grid). The cross-section shown corresponds to the xz plane, and the axes are labeled in units of the gravitational radius. Initially, at $t = 0$, the magnetic field is uniform and vertical. With time, the frozen-in field lines are deformed under the action of the spherically converging accretion flow. The black hole is at the origin.

Fig. 4.— Density distribution in the xz plane in Model A at time $t = 7.88$. The black hole is located at the origin. Matter is concentrated towards the equatorial plane (the horizontal axis) and towards the black hole. Note the density inhomogenities which have been produced by the motion of convective blobs. There is a shock at around $80R_g$, where the supersonically infalling gas from the outer boundary meets the convective core. The two polar funnels are filled with low density matter.

Fig. 5.— Magnetic field lines in the xz plane in Model A at time $t = 7.88$. Except for the polar regions, the magnetic field elsewhere has a highly tangled morphology. This is the result of convection.

Fig. 6.— Velocity streamlines in the xz plane in Model A at time $t = 7.88$. A complicated pattern is seen, with numerous vortices and eddies. This is the result of convection.

This figure "fig2.jpg" is available in "jpg" format from:

http://arXiv.org/ps/astro-ph/0105365v1

This figure "fig3.jpg" is available in "jpg" format from:

http://arXiv.org/ps/astro-ph/0105365v1

This figure "fig4.jpg" is available in "jpg" format from:

http://arXiv.org/ps/astro-ph/0105365v1

This figure "fig5.jpg" is available in "jpg" format from:

http://arXiv.org/ps/astro-ph/0105365v1

This figure "fig6.jpg" is available in "jpg" format from:

http://arXiv.org/ps/astro-ph/0105365v1